

UCLA

UCLA Previously Published Works

Title

SmB6- Cluster Anion: Covalency Involving f Orbitals

Permalink

<https://escholarship.org/uc/item/2z8218ms>

Journal

JOURNAL OF PHYSICAL CHEMISTRY A, 121(8)

ISSN

1089-5639

Authors

Robinson, Paul J
Zhang, Xinxing
McQueen, Tyrel
[et al.](#)

Publication Date

2017

DOI

10.1021/acs.jpca.7b00247

Peer reviewed

This document is confidential and is proprietary to the American Chemical Society and its authors. Do not copy or disclose without written permission. If you have received this item in error, notify the sender and delete all copies.

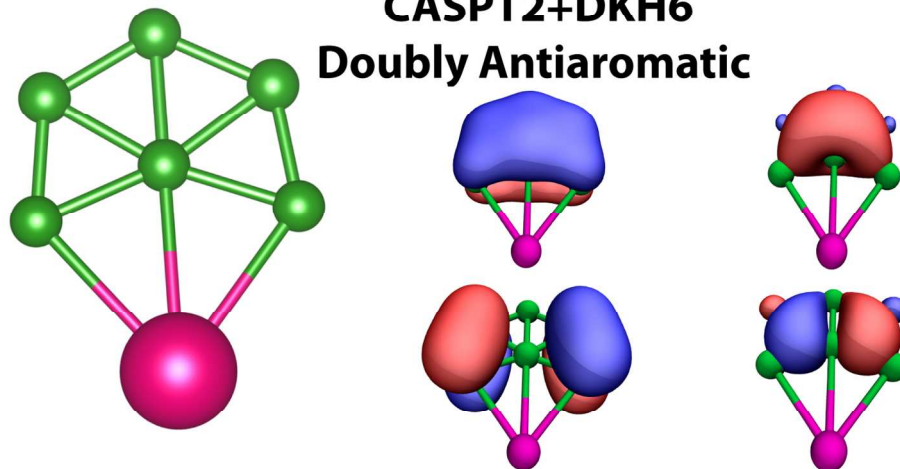
SmB₆⁻ Cluster Anion: Covalency Involving f-Orbitals

Journal:	<i>The Journal of Physical Chemistry</i>
Manuscript ID	jp-2017-00247q.R2
Manuscript Type:	Article
Date Submitted by the Author:	n/a
Complete List of Authors:	Robinson, Paul; University of California, Los Angeles, Chemistry and Biochemistry Zhang, Xinxing; Johns Hopkins University, chemistry McQueen, Tyrel; Johns Hopkins University, Chemistry Bowen, Kit; Johns Hopkins University, Department of Chemistry and Department of Materials Science Alexandrova, Anastassia; University of California, Los Angeles, Chemistry and Biochemistry

SCHOLARONE™
Manuscripts

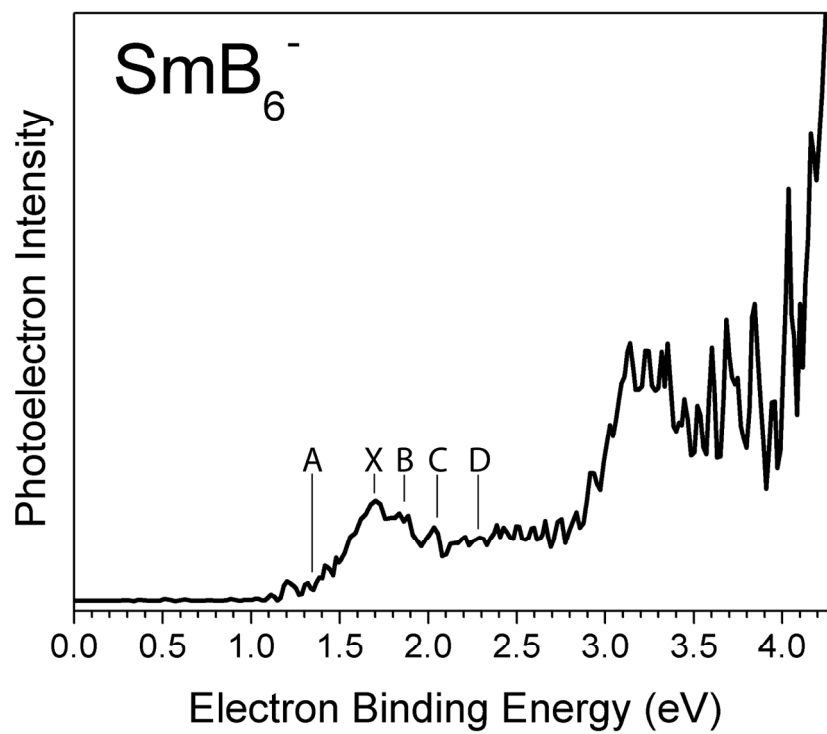
1
2
3
4
5
6
7
8
9
10
11
12
13
14
15
16
17
18
19
20
21
22
23
24
25
26
27
28
29
30
31
32
33
34
35
36
37
38
39
40
41
42
43
44
45
46
47
48
49
50
51
52
53
54
55
56
57
58
59
60

SmB₆⁻
CASPT2+DKH6
Doubly Antiaromatic



TOC Graphics

135x80mm (300 x 300 DPI)



35 Figure 1. The experimental photoelectron spectrum of SmB₆⁻.

36 145x121mm (300 x 300 DPI)

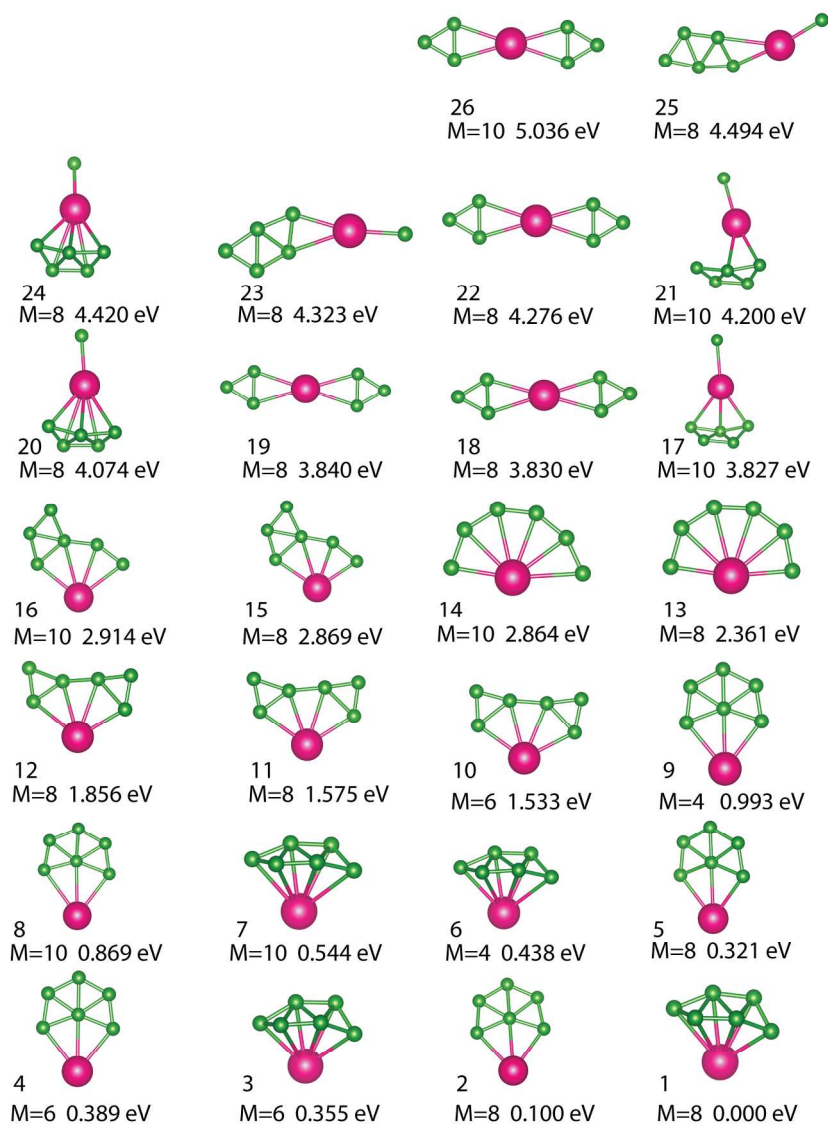


Figure 2. The low-lying minima from a PBE0 global geometry optimization of SmB6-. The energies shown are relative to the lowest energy structure. Because only 0.1 eV separates our lowest two minima, it is necessary to approach this system with higher levels of theory. Symmetry point groups are not identified, because structures resulted from a stochastic global search imposing no symmetry.

161x212mm (300 x 300 DPI)

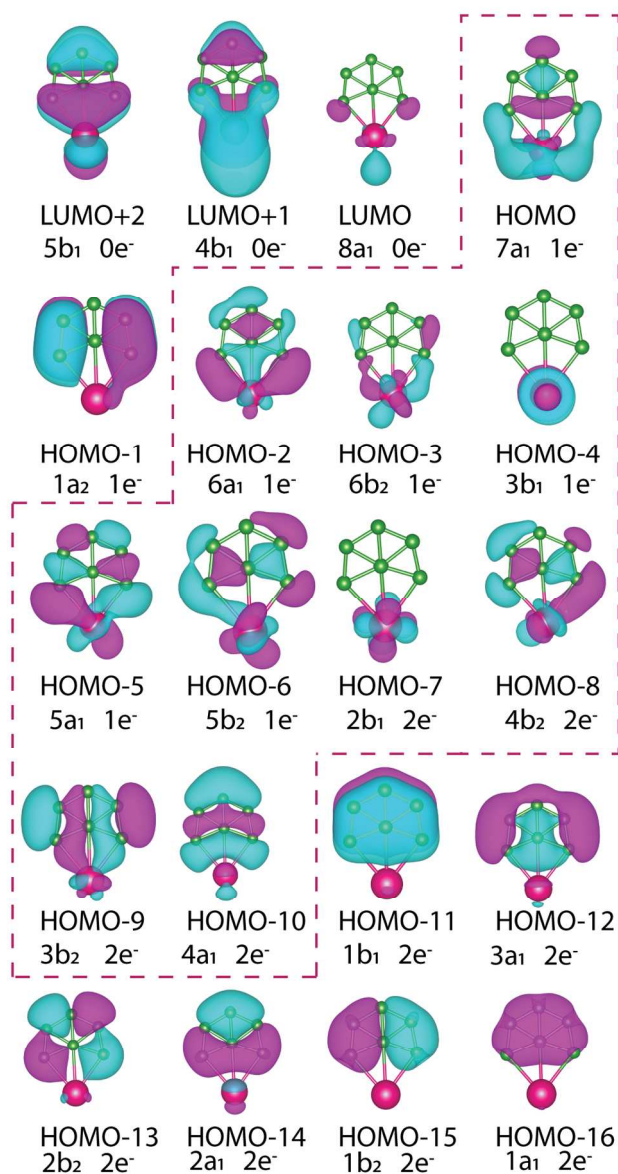


Figure 3. The valence Kohn-Sham orbitals of SmB₆⁻. The outlined orbitals (outlined) contain significant contributions from Sm f-orbitals, according to the expansion of the KS orbitals in terms of atomic orbitals.

94x177mm (300 x 300 DPI)

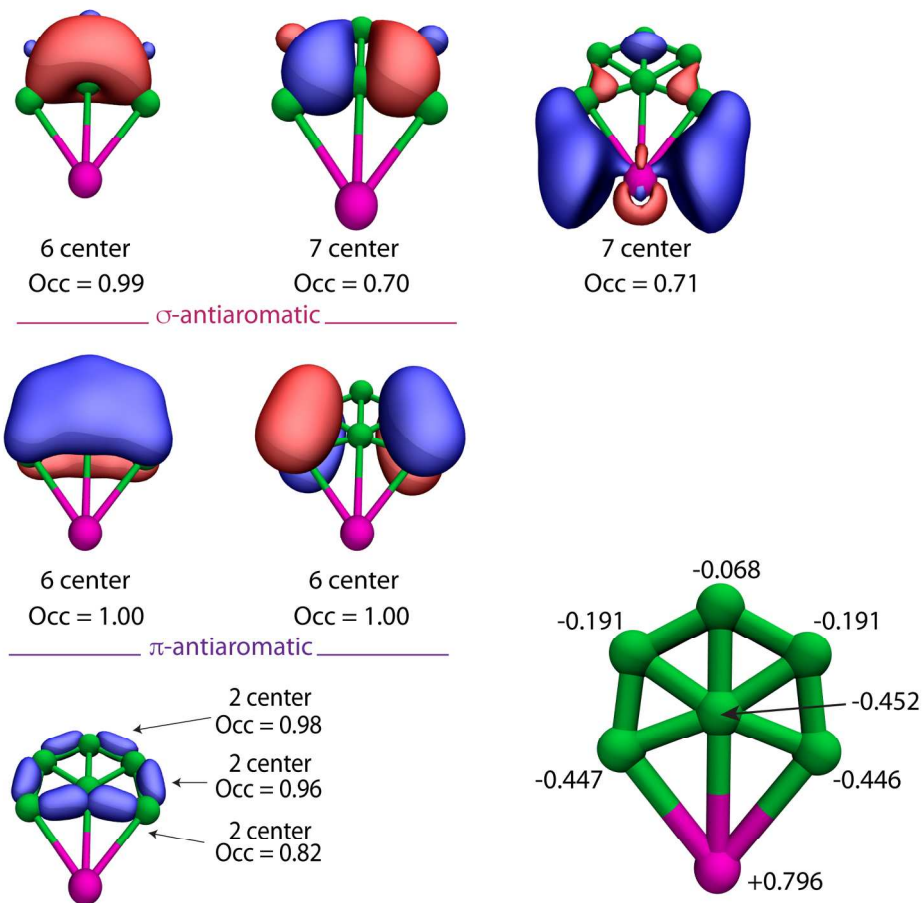


Figure 4. The AdNDP analysis for Smb6-. The annotated cluster in the bottom right shows the Natural Population Analysis charges. Because this is an AdNDP analysis of the alpha density, a fully occupied orbital has an Occ = 1.00. The occupation numbers are the same for each pair of 2 center bonds. Not shown are the 1 center bonds that are simply non-bonding core orbitals on each atom.

171x171mm (300 x 300 DPI)

SmB₆⁻ Cluster Anion: Covalency Involving f-Orbitals

Paul J. Robinson¹, Xinxing Zhang², Tyrel McQueen², Kit H. Bowen*², Anastassia N. Alexandrova*^{1,3}

¹ Department of Chemistry and Biochemistry, University of California, Los Angeles, 607 Charles E. Young Drive East, Los Angeles, CA 90095

² Department of Chemistry and Materials Science, Johns Hopkins University, 3400 N. Charles Street, Baltimore, MD 21218

³ California NanoSystems Institute, 570 Westwood Plaza, Building 114, Los Angeles, California 90095

Corresponding Authors

*kbowen@jhu.edu and ana@chem.ucla.edu

Abstract. While boride clusters of alkali and transition metals have been observed and extensively characterized, so far little is known about lanthanide-boron clusters. Lanthanide boride solids are intriguing, however, and therefore, it is of interest to understand the fundamental electronic properties of such systems, also on the sub-nano scale. We report a joint experimental photoelectron spectroscopic and theoretical study of the SmB₆⁻ anion, iso-stoichiometric to the SmB₆ solid – a topological Kondo insulator. The cluster is found to feature strong static and dynamics electron correlations, and relativistic components, calling for treatment with CASPT2 and up 6th order Douglas-Kroll-Hess (DKH) Relativistic correction. The cluster has a C_{2v} structure, with covalent Sm-B bonds facilitated by f-atomic orbitals on Sm, typically thought to be contracted and inert. Additionally, the cluster retains the double antiaromaticity of the B₆²⁻ cluster.

Introduction

Small Boron clusters are fascinating because they possess a multitude of bonding motifs. In the smallest cluster anions ($B_n^{1/2-}$, $n < 40$) we encounter a diverse group of planar and quasi-planar structures, governed by both strong covalent bonds as well as delocalized (anti)aromatic bonding. For example, B_3^- (D_{3h}) and B_4^- (D_{2h}) are doubly and triply aromatic, respectively.¹ Even with large structures like B_{36} , highly symmetric and aromatic boron structures are favored.² Planarity of these structures is enforced by covalent 2 center – 2 electron (2c-2e) B-B bonds, while the delocalized bonding arrangements dictate the symmetry of the planar structures. On the other hand, the all-boron fullerene, named borospherene, B_{40} , possesses not a single 2c-2e B-B bond, and instead, all the bonds in this species are multicenter.³ This cluster marks a clear difference between the chemistries of boron and its nearest neighbor – carbon. Bulk boron allotropes are three dimensional, and feature a prominent B_{12} icosahedral motif. These boron systems demonstrate the metalloid nature of boron: it will form strong covalent B-B bonds, and also delocalized bonds, of both σ and π -types.^{4,5}

Boron clusters only become more interesting upon the addition of a metal. The metal-like nature of boron allows for an actual metal to weave into an existing aromatic network, leading to high stability. One exciting example of this is $Co@B_8^-$ (D_{8h}), a wheel structure that is aromatic and can be rationalized with the dual nature of boron-the strong covalent bonds between each boron makes the ring stable on the outside, while boron's propensity for delocalized bonding creates an aromatic system containing the central cobalt.⁶ This bonding motif is not an exception; in fact, both ruthenium and tantalum were

1
2
3 shown to form nearly identical wheels with nine and ten borons respectively. Lastly, a
4
5 similar “drum”-looking cluster CoB_{16}^- also shows strong bonds between every two borons,
6
7 in addition to an overall aromaticity of the system.^{7,8} At the same time, small boron clusters
8
9 were shown to serve as possible ligands to metals.⁹ B_8^{2-} and B_6^{2-} both retain their planar
10
11 structure and aromatic/antiaromatic bonding upon coordination to small cations such as
12
13 Li^+ .^{10,11} The boron ligands are anionic in these cases. Thus, boron is promiscuous when
14
15 binding to metals: it can be covalent or anionic, and this property certainly characteristic of
16
17 its metalloid nature. Boron is perfectly matched with d-block metals to form dually
18
19 covalent and aromatic structures, and it is an anion with alkali metals. How would boron
20
21 behave when coordinating lanthanides, for example samarium?
22
23
24
25
26

27 Lanthanides are large atoms (the Sm atom has a covalent radius of 1.98 Å) as
28
29 compared to the tiny second-row boron (0.84 Å in the neutral state).¹² This large difference
30
31 seems to be detrimental to a possible covalent overlap. The possibility of ionic bonding is
32
33 more plausible, due to the difference in electronegativities: 2.04 for B and 1.17 for Sm.
34
35 Indeed, Sm, along with La and Yb, form solid hexaborides, and SmB_6 in particular is a
36
37 topological Kondo insulator,¹³⁻¹⁵ possessing the $\text{Sm}^{2+}/\text{Sm}^{3+}$ mixed valency.¹⁶ In order to
38
39 eventually understand the bonding in these solids, as well as in general in lanthanides-
40
41 boron systems, we begin exploration from the SmB_6^- gas phase anion, stoichiometrically
42
43 identical to the famous SmB_6 solid.
44
45
46
47
48
49
50

51 Experiment

52 The SmB_6^- cluster ion was obtained in the gas phase and its photoelectron spectrum
53
54 was recorded. Anion photoelectron spectroscopy was conducted by crossing a mass-
55
56
57
58
59
60

1
2
3 selected beam of negative ions with a fixed-frequency photon beam and energy-analyzing
4 the resultant photodetached electrons. Our anion photoelectron spectrometer, which has
5 been described previously, consists of a laser vaporization anion source, a linear time-of-
6 flight mass analyzer/selector, a pulsed Nd:YAG photodetachment laser, and a magnetic
7 bottle electron energy analyzer.^{17, 18} Photoelectron spectra were calibrated against the
8 well-known photoelectron spectrum of Cu.¹⁹ Parent anions of SmB₆⁻ were generated in a
9 laser vaporization source. Briefly, a ¼" diameter SmB₆ rod was interrogated by a pulsed
10 Nd:YAG laser beam operating at a wavelength of 532 nm. The resulting plasma was cooled
11 by supersonically expanding a plume of helium gas from a pulsed gas valve (backing
12 pressure of ~150 psi). Negatively charged anions were then extracted into the
13 spectrometer prior to mass selection and photodetachment. The experimental spectrum is
14 shown in Figure 1.
15
16
17
18
19
20
21
22
23
24
25
26
27
28
29
30
31
32
33
34
35
36
37
38
39
40
41
42
43
44
45
46
47
48
49
50
51
52
53
54
55
56
57
58
59
60

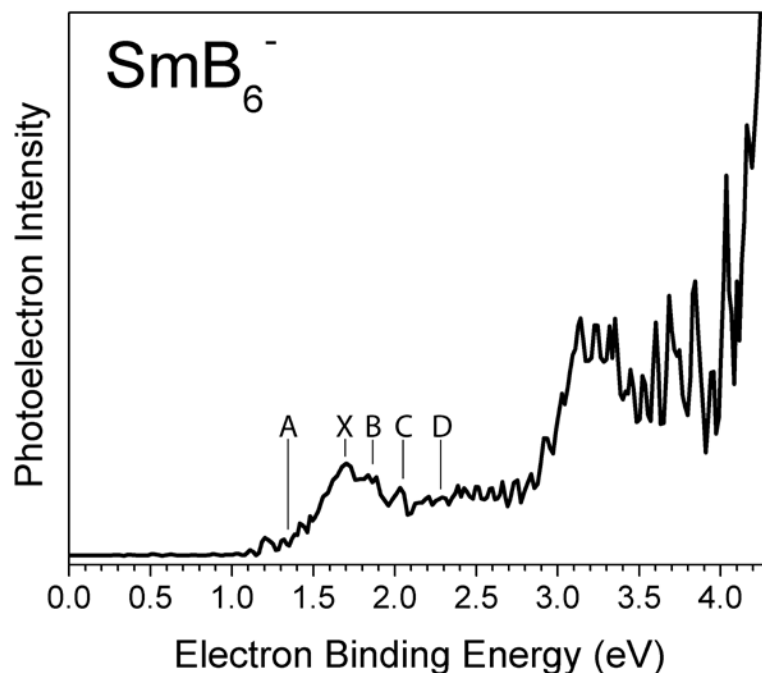


Figure 1. The experimental photoelectron spectrum of SmB_6^- . A, X, B, C and D denote the transitions from the ground state of the anion to the ground and excited states of the neutral.

Theory

Because of the diverse nature of previously observed boron clusters, as well as the oft-counter-intuitive properties of heavy elements like Sm, we do not lean heavily on our chemical intuition in determining the structure of this boride. In fact, a question we wish to answer is whether samarium and lanthanides in general coordinate to boron similarly to other metals. At the same time, the geometric configuration space is vast enough with seven atoms that a little guiding logic is necessary. In general, boron will create bonds with

1
2
3 itself, so we should preference starting seed structures with boron close to itself and in
4
5 groups.
6
7

8 To find the global minimum of SmB_6^- we randomly generated about a hundred
9
10 structures by distributing atoms randomly around the van der Waals radii of the atoms and
11
12 observed which types of structures were likely to converge single point DFT calculations.
13
14 The results of this trial informed our starting structure logic and allowed us to save on
15
16 computation time. Using this, we generated several hundred random structures and
17
18 selected 40 probable starting structures. We included a few non-probable structures to
19
20 minimize our chances of missing a minimum. Each structure was geometry optimized to
21
22 the nearest minimum at the PBE0+ZORA level of theory with the all-electron SARC-ZORA
23
24 basis set on Sm and the 6-31+G* basis on B.²⁰⁻²² PBE0 was chosen because it is known to
25
26 work well for predicting geometries. All the calculations for the optimization were run
27
28 using NWChem 6.5.²³ We optimized each starting structure in four multiplicities: quartet,
29
30 sextet, octet, and decet. We also took each converged minimum and ran a geometry
31
32 optimization of the converged structure in the other multiplets. The lowest 26 minima are
33
34 shown in Figure 2.
35
36
37
38
39
40
41
42
43
44
45
46
47
48
49
50
51
52
53
54
55
56
57
58
59
60

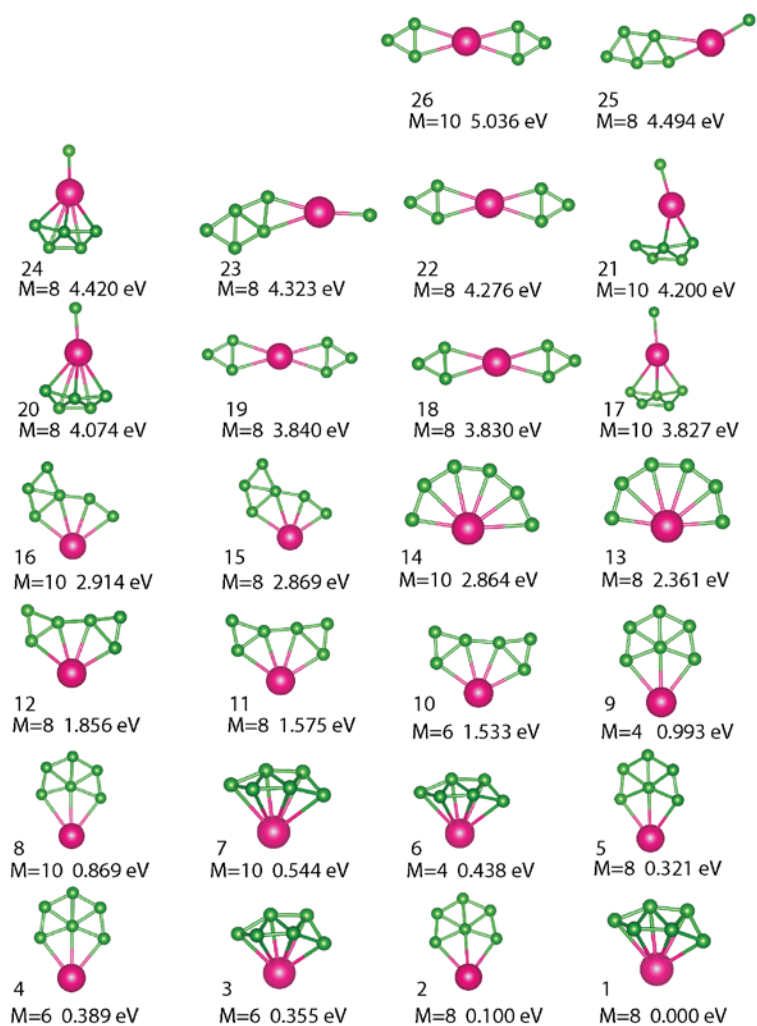


Figure 2. The low-lying minima from a PBE0 global geometry optimization of SmB_6 . The energies shown are relative to the lowest energy structure. M denotes the multiplicity. Because only 0.1 eV separates our lowest two minima, it is necessary to approach this system with higher levels of theory. Symmetry point groups are not identified, because structures resulted from a stochastic global search imposing no symmetry.

The lowest-energy structures are nearly-degenerate octets, of the quasi- C_s and $-C_{2v}$ symmetries. Looking at Figure 2 we see a few motifs repeating throughout the isomer

1
2
3 energy spectrum. For example, the same D_{2h} structure is seen in Figure 2 Numbers 18, 19,
4
5 22 and 26 with two multiplicities and over a range of 1.21 eV. This repetition of nearly
6
7 identical but not energetically degenerate structures is present for all of the low-lying
8
9 isomers including the quasi-degenerate global minima. This is indicative of several features
10
11 of these clusters. First the energy wells by the attached cluster minimum are relatively flat
12
13 with respect to Sm moving around the B_6 unit. This could imply that the boron-samarium
14
15 interaction is a weaker bond than other metal-boron coordination. Additionally, it is
16
17 possible that the small energy differences are an artifact of DFT, and this necessitates
18
19 considering the lowest minima with *ab initio* methods.
20
21
22
23
24

25 The lowest energy structures are all those with all six boron atoms bonded together,
26
27 and the number of B-B bonds roughly correlates with the energy of the isomer. For
28
29 example, the fan-shaped isomer 13 (2.361 eV above the global minimum) is higher in
30
31 energy than the puckered-fan isomer 10 (1.533 eV above the global minimum). Overall, the
32
33 results of the geometry optimization are in line with what we might expect from a boron
34
35 cluster. The energetic stability afforded by all the boron atoms being together is clearly
36
37 present, and the boron networks look much like solitary gas phase boron clusters.
38
39
40
41

42 We will take the DFT optimized geometries, and subject them to higher-level
43
44 treatment, to winnow out which is the actual global minimum and calculate the
45
46 photoelectron spectrum.
47
48

49 Taking the C_{2v} and C_s structures from our global optimization we calculated the
50
51 vertical electron detachment energy by looking at the difference between the energies of
52
53 the octet anion and both the nonet and septet neutral. Unfortunately for DFT, the switch
54
55 from PBE0 to B3LYP and the switch from ZORA to DKH2 both swapped the energetic
56
57
58
59
60

1
2
3 ordering of the isomers. Additionally, the TD-DFT spectra themselves produced negative
4 excitations and were nearly continuous—a clear sign of linear response methods being
5
6 qualitatively incorrect. Along with the likely prospect of state trapping, these problems
7
8
9 with DFT further motivate our need for *ab-initio* methods.
10

11
12
13 To assess what methods would best describe our clusters we performed
14
15 CASSCF(13,16) calculations to determine the multireference character of the two lowest
16
17 minima. Both anions proved to be intrinsically multireference with the Hartree-Fock
18
19 solution having a CI coefficient less than 0.6. The large degree of multireference character
20
21 combined with the large number of electrons in the system informs us that dynamic
22
23 electron correlation needs to be included, and our method of choice for this system is
24
25 CASPT2. For the CASPT2 and initial CASSCF calculations, we selected the all-electron cc-
26
27 pVDZ-DK basis set for B and the cc-pVDZ-DK3 basis set for Sm. We selected a
28
29 CASSCF(11,13) reference calculation as the starting point for all of our PT2 calculations. To
30
31 aid in convergence, a level-shift of 0.3 was applied to all PT2 calculations. All *ab initio*
32
33
34
35
36
37 calculations were performed with Molpro 2015.^{24, 25}
38

39
40 Because the photoelectron spectrum requires a high degree of accuracy for the
41
42 relativistic corrections, we need to benchmark the Relativistic Douglas-Kroll-Hess (DKH)
43
44 approximation for this system.²⁶ While ZORA was sufficient for the geometry optimization,
45
46 we use DKH for the single point calculations because it offers a tunable accuracy. In the
47
48 limit of infinite order, the DKH approaches the exact spin-free electron-only Dirac
49
50 Hamiltonian. In most applications the second order is sufficient to capture the scalar
51
52 relativistic effects and is considered the standard. We found that at the second order
53
54
55
56
57 neither the absolute energies of the anion and neutral species, nor the energy differences
58
59
60

1
2
3 between the two were reliable (Table 1). We needed to go to the 6th order DKH before the
4 absolute energy of the anion stabilized sufficiently. The energy differences between the
5 neutrals and the anion began to converge by the 4th order DKH, but we chose to run all our
6 *ab initio* spectrum calculations at the 6th order for added assurance and accuracy. The
7 energy differences reported in Table 1 are not unreasonably large: in the original paper
8 describing the arbitrary order DKH method by Reiher et al, the change in energy between
9 DKH2 and DKH4 for a single gold atom was -370eV.²⁷ It must also be noted that the DKH
10 approximation is spin-free; however, spin-orbit coupling should not be an issue for the low
11 lying excitations in this cluster because the adjacent spin states are far apart in energy.
12
13
14
15
16
17
18
19
20
21
22
23

24
25 With CASPT2+DKH6, we find that the octet C_{2v} isomer is the lowest energy
26 structure, beating out the octet C_s by a 0.24 eV. We can now solely consider the C_{2v}
27 structure for the purposes of determining the bonding and photoelectron spectrum.
28
29
30
31
32
33
34

35 Results and Discussion

36
37 **Table 1:** The relative energy of the C_{2v} anion with respect to the DKH2. The second order is
38 entirely insufficient and misses a large amount of the relativistic energy. By the 4th order it
39 has recovered enough of the energy to generate excitations within the 0.1eV experimental
40 error. * No convergence was obtained for DKH8 on the neutrals.
41
42
43
44
45

DKH Order	Energy (eV)	VDE (eV)
DKH2	0.0	2.53
DKH4	-125.6	1.70
DKH6	-129.4	1.75

DKH8	-129.8	*
------	--------	---

1
2
3
4
5
6
7
8 The first VDE (feature X, Figure 1 and Table 2) to the septet was calculated to be
9 1.75 eV, in agreement with the 1.70 ± 0.1 eV experimentally observed VDE. The
10 corresponding Adiabatic Detachment Energy (ADE) was calculated by PBE0 optimizing the
11 septet, exactly as we did for the global optimization, and then running a CASPT2+DKH6
12 single point. The calculated ADE (A) of 1.43 eV was also in agreement with experimental
13 ADE of 1.35 ± 0.1 eV. Another feature (B) corresponds to a photodetachment to an excited
14 state septet and is calculated to be 1.85 eV in agreement with the experimental 1.85 ± 0.1 eV.
15 Past the shoulder, a small peak (C) was shown to be yet another detachment to a final
16 excited septet state. The experimental and the theoretical values, 2.05 ± 0.1 eV and 1.97 eV,
17 respectively, coincide. Finally, the detachment to a nonet, 9A_2 , (D) was calculated to be 2.31
18 eV and corresponds to a not-fully-resolved peak in a very populated area of the spectrum.
19 The density of excited states past feature D is such that we cannot assign meaningful
20 transitions to each peak or, in fact, even distinguish them from experimental error or each
21 other. The pile up of so many excited septet states and nonet states will make the SO
22 coupling non-ignorable and intractable. All data past 2.5 eV can be seen as many excitations
23 on top of one another.
24
25
26
27
28
29
30
31
32
33
34
35
36
37
38
39
40
41
42
43
44
45
46
47
48
49
50
51
52
53
54
55
56
57
58
59
60

Table 2. The CASPT2+DKH6 excitation energies from the septet neutral. The spectroscopic states are taken from the Kohn-Sham orbitals and the largest weighted CI coefficient. 8B_2 is defined as the ground state. The differences between the experiment and theory are well within the experimental error and the expected variance of DKH6.

Label	State	Calculated Energy (eV)	Experimental Energy (eV)
	8B_2	0.00 eV	0.00 eV
A	7B_2 ADE	1.43 eV	1.35 ± 0.1 eV
X	7B_2 VDE	1.75 eV	1.70 ± 0.1 eV
B	7B_2	1.85 eV	1.85 ± 0.1 eV
C	7B_2	1.97 eV	2.05 ± 0.1 eV
D	9A_2	2.31 eV	2.30 ± 0.1 eV

As will be shown in the next section, all of the lowest energy spectral features correspond to the photodetachment channels from the B_6 -unit in the cluster, as the highest occupied orbitals are centered on boron and involve minimally the contributions from Sm. Considering that (i) the binding of Sm to the boron cluster is weak, (ii) the B_6 structure in several low-energy isomers of SmB_6^- is preserved, (iii) many isomers are within a small energy-range from the global minimum at varying levels of theory, and (iv) the lowest channels in the spectrum correspond to the photodetachment from boron, we are forced to suspect that several isomers of SmB_6^- could produce similar spectra in agreement with the experiment. Thus, in this case, the agreement with the experiment is possibly not fully assuring of the structure. Our C_{2v} structure is produced at the highest level of theory possible today, and the agreement with the experiment is great; yet we opt to leave this

1
2
3 structure as a proposal. We are confident to state, however, that the experimentally
4
5 observed isomer or isomers should contain a connected boron cluster, with the highest
6
7 occupied MOs belonging to boron.
8
9

10 To understand the bonding in this cluster we first look at the Kohn-Sham orbitals of
11
12 the octet anion (Figure 3). In general, the delocalized boron bonding stays intact as it would
13
14 be found in the B_6^{2-} cluster. This is seen particularly well in the lowest energy orbitals: $1a_1$
15
16 $1b_2$ $2a_1$ and $2b_2$ form a sigma bonding and antibonding system, and $3a_1$ $4a_1$ $3b_2$ and $4b_2$
17
18 from a peripheral sigma bonding and antibonding system. There is also clearly a π -
19
20 antiaromatic system composed of $1b_1$ and $1a_2$. By employing a Natural Population Analysis
21
22 (NPA) we see that the B_6 portion of SmB_6^- carries a -1.796 charge, meaning it is close in
23
24 electronic structure to the B_6^{2-} cluster. The charge of +0.796 on Sm is approximately the
25
26 Sm(I) oxidation state. The difference between the -2 anion of B_6 and the +1 cation of Sm is
27
28 shared between the two units in the form of covalent bonds, which we will further examine.
29
30
31
32
33
34
35
36
37
38
39
40
41
42
43
44
45
46
47
48
49
50
51
52
53
54
55
56
57
58
59
60

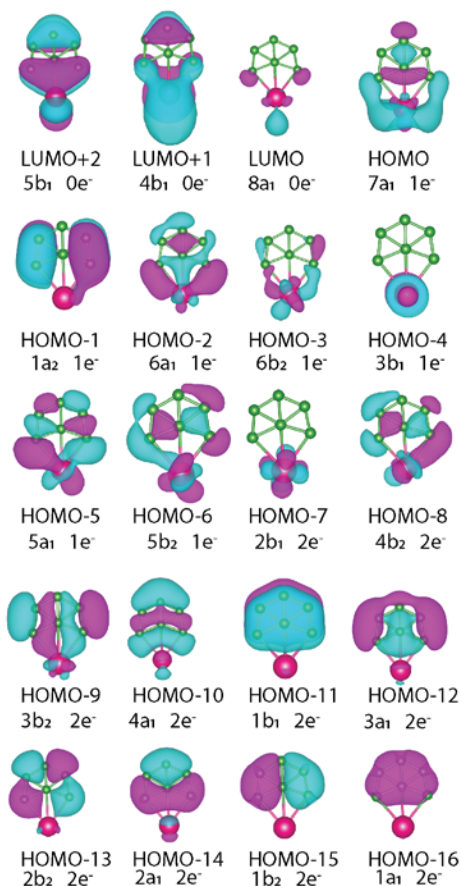


Figure 3. The valence and lowest energy unoccupied Kohn-Sham orbitals of SmB_6 . Clearly present are the aromatic and delocalized bonding motifs seen in the isolated B_6 cluster. Interestingly, the f-orbitals are shown to have significant overlap with the sigma antibonding systems

The higher energy orbitals of SmB_6 also show delocalized boron bonding, but there the Sm f-orbitals and d-orbitals have a significant overlap with the delocalized sigma antibonding orbitals. This is somewhat similar to previous reports of metals binding to boron clusters.²⁸ With LaB_n clusters, the d-orbitals join into the p-orbital networks. Additionally, in TaB_6 the predicted geometry is the same as SmB_6 and it possesses a similar bonding

1
2
3 scheme.²⁹ The similarity in structure between TaB₆⁻ and SmB₆⁻ suggests that SmB_n⁻ (n>10)
4
5 clusters might form wheels with even higher coordination numbers than Ta. However, both
6
7 the TaB₆⁻ and the LaB_n⁻ clusters are vastly different from the SmB₆⁻ cluster because no
8
9 multireference character was necessary to reproduce the spectrum (both papers used the
10
11 inherently single reference CCSD(T)). The major bonding difference is that here we have f-
12
13 orbitals participating directly in the valence bonding, which is unusual because of their
14
15 relativistic contraction. Sm is in the perfect spot on the periodic behavior to observe this
16
17 bonding because its f-orbitals are the least contracted of the lanthanide series due to their
18
19 high population. Because of the participation of the f and d orbitals in the bonding it
20
21 becomes difficult to assess the bonding types present in the remaining orbitals. For this
22
23 situation, the Adaptive Natural Density Partitioning (AdNDP) analysis is indispensable.³⁰
24
25
26
27
28
29

30 An AdNDP analysis is helpful in determining what types of bonds actually result
31
32 from the calculated alpha electron density. Using the alpha density means the maximum
33
34 occupation of our bonds is 1.00. Our AdNDP analysis localized 2 center-2 electron (Lewis)
35
36 bonds between the perimeter borons (Figure 4), with good occupation numbers of 0.98 e⁻
37
38 0.98 e⁻ 0.96 e⁻ 0.96 e⁻ 0.82 e⁻ and 0.82 e⁻. It also recovers the delocalized antiaromatic
39
40 system seen in 1a₂ and 1b₁. These are both fully occupied with 1.00 e⁻ each. By checking
41
42 this result against the KS-orbitals, we note that the delocalized π-system contains a total of
43
44 3 electrons, a pair in the HOMO-11, and a single electron in the HOMO-1, since the system is
45
46 an octet. Hence, in this situation, the Hückel's electron-counting rule of 4n for antiaromatic
47
48 compounds does not hold up, but the antiaromaticity can nevertheless be claimed.
49
50 Additionally, AdNDP finds an antiaromatic σ-system from the remaining electron density.
51
52 This system also has good electron counts of 0.99 and 0.70 e⁻. Therefore, we can classify the
53
54
55
56
57
58
59
60

C_{2v} as doubly antiaromatic, σ - and π -. Double antiaromaticity was observed also in the B_6^- cluster ion in isolation, although its planar structure is slightly different. In addition to both of the antiaromatic networks, there remains a peripheral Sm-B bond of a_1 symmetry (σ -type). This bond is composed of p-orbitals on boron and both f- and d-orbitals on Sm and has an occupation of 0.71 e^- . The presence of bonding f-orbitals, even in a hybrid, is novel, since f-orbitals are normally considered too contracted to play any role in valence states. This observation brings f-orbitals into the fray. The way Sm binds to the boron cluster is reminiscent of how d-block elements bind to boron, except the latter use d-orbitals, whereas Sm heavily involves f-orbitals as well.

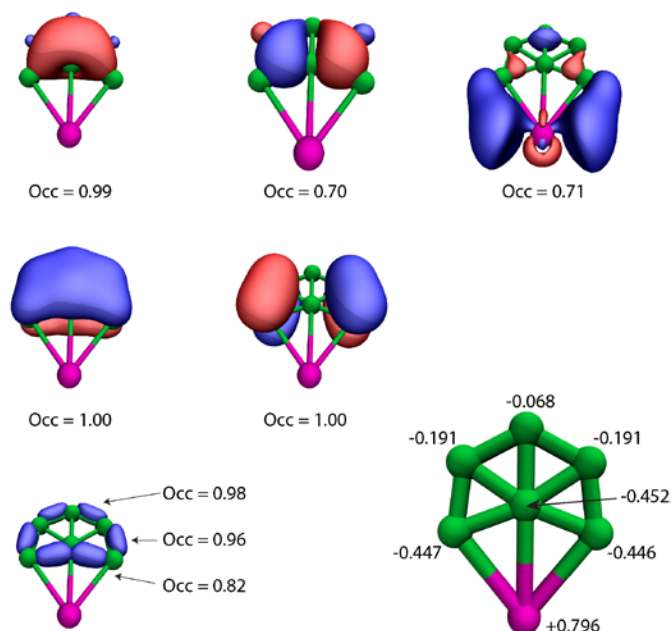


Figure 4. The AdNDP analysis for SmB_6^- . The annotated cluster in the bottom right shows the Natural Population Analysis charges. Because this is an AdNDP analysis of the alpha density, a fully occupied orbital has an $Occ = 1.00$. The lower left bonds are the 6 $2c-2e$ bonds joining the peripheral borons. The occupation numbers are the same for each pair of

1
2
3 bonds. The middle left two bonds show the π -antiaromatic system. The top two bonds on
4
5 the left are the σ -antiaromatic system. The top right bond is the peripheral sigma Sm-B
6
7 bond. Not shown are the 1c-2e bonds that are simply non-bonding core orbitals on each
8
9 atom.
10
11

12 13 14 15 16 **Conclusion**

17
18 We showed that SmB_6^- is an incredibly sensitive system possessing relativistic
19
20 effects and electron correlation thoroughly outside the realm of go-to DFT treatments and
21
22 single reference methods. In order to accurately reproduce the experimental photoelectron
23
24 spectrum, this system required a *tour de force* of computational chemistry's finest methods:
25
26 excited state CASPT2 and 6th order relativistic effects. The only area where we retain
27
28 confidence in DFT for this system is in predicting the geometries. Far from only being a
29
30 challenging quantum mechanical puzzle, SmB_6^- also possesses fascinating bonding
31
32 properties. AdNDP analysis shows that its C_{2v} structure retains the double antiaromaticity
33
34 of B_6^{2-} and also incorporates f orbitals into a Sm-B covalent bond. This recruitment of f-
35
36 orbitals into the bonding fray opens up the possibility of designing larger clusters with
37
38 never-before-seen bonding motifs.
39
40
41
42
43

44 45 **Acknowledgments**

46
47 This work was supported by the Air Force Office of Scientific Research (AFOSR) under
48
49 Grant No. FA9550-15-1-0259 (K.H.B.), FA9550-16-1-0141 (A.N.A.), NSF Career Award No.
50
51 CHE1351968 (A.N.A.), and the generous donation of Ms. Evers-Manly as part of the
52
53 Undergraduate Research Scholars Program of the UCLA Undergraduate Research Center-
54
55 Sciences (P. J. R.). UCLA IDRE cluster Hoffman2 was used for all calculations.
56
57
58
59
60

References

1. Zhai, H.-J.; Wang, L.-S.; Alexandrova, A. N.; Boldyrev, A. I.; Zakrzewski, V. G., Photoelectron Spectroscopy And Ab Initio Study Of B_3^- And B_4^- Anions And Their Neutrals. *J. Phys. Chem. A* **2003**, *107*, 9319--9328.
2. Piazza, Z. A.; Hu, H. S.; Li, W. L.; Zhao, Y. F.; Li, J.; Wang, L. S., Planar Hexagonal B(36) As A Potential Basis For Extended Single-Atom Layer Boron Sheets. *Nat. Commun.* **2014**, *5*, 3113.
3. Zhai, H. J.; Zhao, Y. F.; Li, W. L.; Chen, Q.; Bai, H.; Hu, H. S.; Piazza, Z. A.; Tian, W. J.; Lu, H. G.; Wu, Y. B., et al. Observation Of An All-Boron Fullerene. *Nat. Chem.* **2014**, *6*, 727-31.
4. Oger, E.; Crawford, N. R.; Kelting, R.; Weis, P.; Kappes, M. M.; Ahlrichs, R., Boron Cluster Cations: Transition From Planar To Cylindrical Structures. *Angew. Chem. Int. Ed.* **2007**, *46*, 8503-8506.
5. Wang, L.-S., Photoelectron Spectroscopy Of Size-Selected Boron Clusters: From Planar Structures To Borophenes And Borospherenes. *Int. Rev. Phys. Chem* **2016**, *35*, 69-142.
6. Romanescu, C.; Galeev, T. R.; Li, W.-L.; Boldyrev, A. I.; Wang, L.-S., Transition-Metal-Centered Monocyclic Boron Wheel Clusters ($M@B_n$): A New Class of Aromatic Borometallic Compounds. *Acc. Chem. Res.* **2013**, *46*, 350-358.
7. Jian, T.; Li, W.-L.; Popov, I. A.; Lopez, G. V.; Chen, X.; Boldyrev, A. I.; Li, J.; Wang, L.-S., Manganese-Centered Tubular Boron Cluster – MnB_{16}^- : A New Class Of Transition-Metal Molecules. *J. Chem. Phys.* **2016**, *144*, 154310

- 1
2
3
4
5
6
7
8
9
10
11
12
13
14
15
16
17
18
19
20
21
22
23
24
25
26
27
28
29
30
31
32
33
34
35
36
37
38
39
40
41
42
43
44
45
46
47
48
49
50
51
52
53
54
55
56
57
58
59
60
8. Popov, I.; Jian, T.; Lopez, G.; Boldyrev, A.; Wang, L., Cobalt-Centred Boron Molecular Drums With The Highest Coordination Number In The CoB_{16}^- Cluster. *Nat. Commun.* **2015**, *6*.
 9. Alexandrova, A. N.; Boldyrev, A. I.; Zhai, H.-J.; Wang, L.-S., All-Boron Aromatic Clusters As Potential New Inorganic Ligands And Building Blocks In Chemistry. *Coord. Chem. Rev.* **2006**, *250*, 2811-2866.
 10. Alexandrova, A. N.; Boldyrev, A. I.; Zhai, H.-J.; Wang, L.-S.; Steiner, E.; Fowler, P. W., Structure And Bonding In B_6^- And B_6 : Planarity And Antiaromaticity. *J. Phys. Chem. A* **2003**, *107*, 1359-1369.
 11. Alexandrova, A. N.; Zhai, H.-J.; Wang, L.-S.; Boldyrev, A. I., Molecular Wheel B_8^{2-} As A New Inorganic Ligand. Photoelectron Spectroscopy And Ab Initio Characterization Of LiB_8 . *Inorg. Chem.* **2004**, *43*, 3552--3554.
 12. Cordero, B.; Gómez, V.; Platero-Prats, A. E.; Revés, M.; Echeverría, J.; Cremades, E.; Barragán, F.; Alvarez, S., Covalent Radii Revisited. *J. Chem. Soc., Dalton Trans.* **2008**, 2832-2838.
 13. Dzero, M.; Sun, K.; Galitski, V.; Coleman, P., Topological Kondo Insulators. *Phys. Rev. Lett.* **2010**, *104*, 106408
 14. Cooley, C.; Aronson, M.; Fisk, Z.; Canfield, P., SmB_6 - Kondo Insulator Or Exotic Metal. *Phys. Rev. Lett.* **1995**, *74*, 1629-1632.
 15. Neupane, M.; Alidoust, N.; Xu, S.; Kondo, T.; Ishida, Y.; Kim, D.-J.; Liu, C.; Belopolski, I.; Jo, Y.; Chang, T.-R., Surface Electronic Structure Of The Topological Kondo-Insulator Candidate Correlated Electron System SmB_6 . *Nat. Commun.* **2013**, *4*.
 16. Antonov, V. N.; Shpak, A. P.; Yaresko, A. N., Electronic Structure Of Mixed Valent

1
2
3 Systems. *Condens. Matter Phys.* **2004**, *7*, 211-246.

4
5
6 17. Zhang, X.; Wang, Y.; Wang, H.; Lim, A.; Gantefoer, G.; Bowen, K. H.; Reveles, J. U.;

7
8 Khanna, S. N., On The Existence Of Designer Magnetic Superatoms. *J. Am. Chem. Soc.* **2013**,
9
10 *135*, 4856-4861.

11
12
13 18. Zhang, X.; Robinson, P.; Gantefor, G.; Alexandrova, A.; Bowen, K., Photoelectron
14
15 Spectroscopic And Theoretical Study Of The [HPd(η^2 -H₂)]⁻ Cluster Anion. *J. Chem. Phys.*
16
17 **2015**, *143*, 094307

18
19
20 19. Ho, J.; Ervin, K. M.; Lineberger, W. C., Photoelectron Spectroscopy Of Metal Cluster
21
22 Anions: Cu_n⁻, Ag_n⁻, And Au_n⁻. *J. Chem. Phys.* **1990**, *93*, 6987-7002.

23
24
25 20. Adamo, C.; Barone, V., Toward Reliable Density Functional Methods Without
26
27 Adjustable Parameters: The PBE0 Model. *J. Chem. Phys.* **1999**, *110*, 6158-6170.

28
29
30 21. Pantazis, D.; Neese, F., All-Electron Scalar Relativistic Basis Sets for the Lanthanides.
31
32 *J. Chem. Theory Comput.* **2009**, *5*, 2229-2238.

33
34
35 22. Francl, M. M.; Pietro, W. J.; Hehre, W. J.; Binkley, J. S.; Gordon, M. S.; DeFrees, D. J.;

36
37 Pople, J. A., Self-Consistent Molecular Orbital Methods. XXIII. A Polarization-Type Basis Set
38
39 For Second-Row Elements. *J. Chem. Phys.* **1982**, *77*, 3654-3665.

40
41
42 23. Valiev, M.; Bylaska, E.; Govind, N.; Kowalski, K.; Straatsma, T.; Van Dam, H.; Wang, D.;

43
44 Nieplocha, J.; Apra, E.; Windus, T., et al , NWchem: A Comprehensive And Scalable Open-
45
46 Source Solution For Large Scale Molecular Simulations. *Comput. Phys. Commun.* **2010**, *181*,
47
48 1477-1489.

49
50
51 24. Celani, P.; Werner, H.-J., Multireference Perturbation Theory For Large Restricted
52
53 And Selected Active Space Reference Wave Functions. *J. Chem. Phys.* **2000**, *112*, 5546-5557.

- 1
2
3
4
5
6
7
8
9
10
11
12
13
14
15
16
17
18
19
20
21
22
23
24
25
26
27
28
29
30
31
32
33
34
35
36
37
38
39
40
41
42
43
44
45
46
47
48
49
50
51
52
53
54
55
56
57
58
59
60
25. Werner, H.-J.; Knowles, P. J.; Knizia, G.; Manby, F. R.; Schütz, M., Molpro: A General-Purpose Quantum Chemistry Program Package. *Wiley. Interdiscip. Rev. Comput. Mol. Sci.* **2012**, *2*, 242-253.
26. Liu, W.; Peng, D., Infinite-Order Quasirelativistic Density Functional Method Based On The Exact Matrix Quasirelativistic Theory. *J. Chem. Phys.* **2006**, *125*, 044102.
27. Reiher, M.; Wolf, A., Exact Decoupling Of The Dirac Hamiltonian. II. The Generalized Douglas–Kroll–Hess Transformation Up To Arbitrary Order. *J. Chem. Phys.* **2004**, *121*, 10945-10956.
28. Cheng, S.-B.; Berkdemir, C.; Castleman, A., Observation Of d–p Hybridized Aromaticity In Lanthanum-Doped Boron Clusters. *Phys. Chem. Chem. Phys.* **2014**, *16*, 533-539.
29. Li, W.-L.; Ivanov, A. S.; Federič, J.; Romanescu, C.; Černušák, I.; Boldyrev, A. I.; Wang, L.-S., On The Way To The Highest Coordination Number In The Planar Metal-Centred Aromatic Ta@B₁₀- Cluster: Evolution Of The Structures Of TaB_n⁻ (N= 3–8). *J. Chem. Phys.* **2013**, *139*, 104312.
30. Zubarev, D. Y.; Boldyrev, A. I., " Developing Paradigms Of Chemical Bonding: Adaptive Natural Density Partitioning. *Phys. Chem. Chem. Phys.* **2008**, *10*, 5207-5217.

1
2
3
4
5
6
7
8
9
10
11
12
13
14
15
16
17
18
19
20
21
22
23
24
25
26
27
28
29
30
31
32
33
34
35
36
37
38
39
40
41
42
43
44
45
46
47
48
49
50
51
52
53
54
55
56
57
58
59
60

TOC Graphic:

